Materials Advances

ROYAL SOCIETY OF CHEMISTRY

PAPER

View Article Online
View Journal | View Issue

Cite this: *Mater. Adv.*, 2025, **6**, 7505

Dysprosium(III) complexes as potential near-white light emitters: a comprehensive study on the influence of coordination environment

Sofia Malik,[a] Komal Jakhar,†*[a] Devender Singh, †*[a] Swati Dalal,[a] Vandana Aggarwal,[a] Sumit Kumar,[b] Parvin Kumar[c] and Jayant Sindhu [d]

Received 12th June 2025,
Accepted 7th September 2025

DOI: 10.1039/d5ma00632e

rsc.li/materials-advances

The coordination of both beta-diketonate and neutral ligands to Dy(III) ions, using a one-pot room temperature synthesis, yielded a series of UV-sensitized luminescent complexes. Specifically, $[Dy(BBA)_3(bpy)]$, $[Dy(BBA)_3(phen)]$, $[Dy(BBA)_3(brphen)]$ and $[Dy(BBA)_3(neo)]$ were obtained, demonstrating efficient UV to Visible conversion. The strategic assembly of 1-(4-bromophenyl)butane-1,3-dione (BBA) and various neutral ligands around the Dy(III) ions resulted in the formation of a protective coordination environment. This environment significantly enhances the luminescence properties, leading to high luminescence intensity and extended emission lifetimes with white emission. A comprehensive analysis of the composition, thermal stability and photophysical properties of these Dy(III) complexes was conducted using FT-IR, NMR, UV-vis, PL and thermal techniques. The structure of the ancillary moieties played an important role in determining the emission characteristics of these Dy(III) coordination complexes, which were found to be thermally stable. The branching ratio, which is a critical parameter for laser design, was also calculated. Additionally, the semiconducting properties, CIE color coordinates and correlated color temperature values were also evaluated.

1. Introduction

In the context of expanding global energy needs and growing environmental concerns, the pursuit of sustainable energy solutions has driven significant advancements across various fields. The rapid evolution of solid-state lighting (SSL) materials has been fuelled by this growing global demand for energy. These are not only significantly more efficient than incandescent lamps, but also offer enhanced environmental compatibility relative to traditional fluorescent and mercury lamps. Among these materials, solid-state white light emitting materials have garnered significant attention from researchers owing to their long operational lifetime and energy saving efficiency with a wide range of applications ranging from mood-sensitive lighting to large-panel displays.[1–4] SSL sources may be differentiated according to their material composition, comprising inorganic phosphors (LEDs) or organic molecular semiconductors (OLEDs) and their excitation mechanism, employing ultraviolet stimulation (LEDs) or electrical stimulation (OLEDs).[5] White light emission (WLE) can be obtained either *via* a dichromatic emitter [blue and yellow (B/Y) or blue and red (B/R)] or *via* combining the three primary colors (RGB). But, the use of physical mixing of primary colors for white-light generation presents challenges related to phase separation and stability, which can restrict their applications. In contrast to traditional mixing methods, single-component systems offer superior stability and reproducibility, and eliminate phase separation, leading to simpler fabrication.[6] Furthermore, white-light emission can also be achieved from single molecules which cover the whole visible spectrum. Single-molecule systems simplify device fabrication by providing a stable, single-phase, single-emitter source.[7] In the search for stable and efficient single-component WLE systems, lanthanide complexes have also sparked significant interest on account of their well-defined emissive profiles, long-lived excited states and large Stokes shifts, which is primarily because of their f–f electronic transitions. These transitions are minimally influenced by the surrounding environment, resulting in high color purity and narrow emission bands, which are advantageous for high-resolution imaging and display technologies.[8] But due to parity selection rules, these transitions are forbidden leading to inherently low absorption coefficients making direct excitation of lanthanide ions difficult.[9]

It is well-established that the luminescence of trivalent lanthanide ions can be enhanced *via* indirect excitation, *i.e.*

[a] *Department of Chemistry, Maharshi Dayanand University, Rohtak, 124001, Haryana, India*
[b] *Department of Chemistry, DCR University of Science and Technology, Murthal, 131039, Haryana, India*
[c] *Department of Chemistry, Kurukshetra University Kurukshetra, 136119, Haryana, India*
[d] *Department of Chemistry, COBS&H, CCS Haryana Agricultural University, Hisar, 125004, Haryana, India*
† These authors contributed equally to this work.

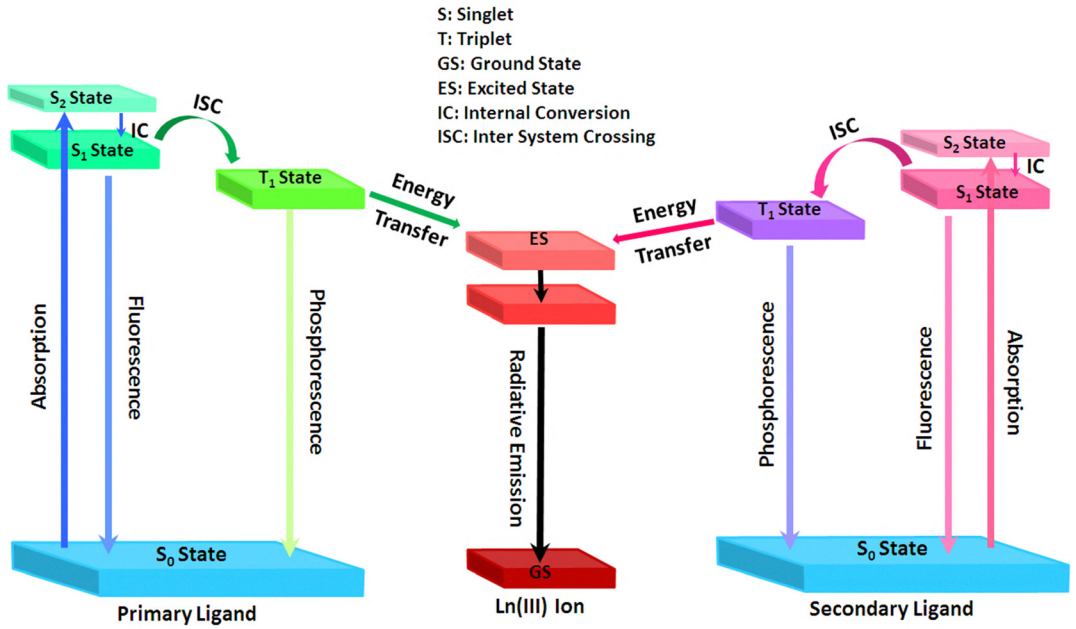

Fig. 1 Jablonski diagram illustrating ligand-mediated excitation and energy transfer.

the antenna effect (Fig. 1), where organic antenna chromophores are often used to enhance luminescence through energy transfer.[10] β-Diketone ligands are known to be excellent complexing agents for lanthanide ions (Ln^{3+}) for several reasons: (a) their strong absorption across a broad wavelength range (due to π–π* transitions), making them ideal sensitizers for luminescence by Ln^{3+} ions; (b) they form strong adducts with lanthanide ions; (c) the resulting β-diketonate lanthanide complexes are sufficiently stable for practical applications.[11,12] Tris β-diketonate lanthanide complexes typically possess an unsaturated coordination sphere, leading to the incorporation of coordinated solvent ligands rich in high-energy oscillators like C–H and O–H vibrations.[13] These oscillators promote non-radiative energy loss from the excited states of the lanthanide ion. To mitigate this solvent quenching, neutral ancillary ligands like 2,2′-bipyridine (bpy) or 1,10-phenanthroline (phen) are commonly employed to saturate the inner coordination sphere.[14,15] These ancillary ligands can also enhance the sensitization of the Ln^{3+} ion if their energy levels are suitable for efficient energy transfer.

One approach to achieve white light emission through lanthanide ions involves utilizing the characteristic emission of the trivalent dysprosium ion. When exposed to ultraviolet light, Dy(III) ions ($4f^9$ configuration) emit sharp bands at 480, 572 and 650 nm, corresponding to $^4F_{9/2}$ to $^6H_{15/2}$, $^6H_{13/2}$ and $^6H_{11/2}$ transitions.[16,17] These emissions manifest as blue, yellow and red fluorescence, respectively. The path connecting yellow and blue wavelengths in the CIE 1931 chromaticity diagram usually intersects in the white light region. Additionally, hypersensitive transition intensity varies more noticeably with environmental factors. Therefore, altering the yellow-to-blue intensity ratio by modifying the ligands and coordination environment can produce white luminescence.[18] Recent studies have highlighted the potential of lanthanide-based complexes for white-light generation and device fabrication,[19–21] yet a detailed understanding of how structural modification of neutral ancillary ligands influences the photophysical behavior of Dy(III) complexes remains limited. This knowledge gap motivates the present study, which systematically explores the impact of four neutral ligands 2,2′-bipyridine (bpy), 1,10-phenanthroline (phen), 2,9-dibromo-1,10-phenanthroline (brphen) and 2,9-dimethyl-1,10-phenanthroline (neo) on the photophysical properties of ternary trivalent dysprosium complexes. Using these ligands as ancillary ligands, BBA as the primary ligand and the Dy(III) ion as the emissive center, four complexes were synthesized, namely $[Dy(BBA)_3bpy]$ (**D1**), $[Dy(BBA)_3phen]$ (**D2**), $[Dy(BBA)_3brphen]$ (**D3**) and $[Dy(BBA)_3neo]$ (**D4**). The synthesized complexes were further characterized *via* thermal analysis, FT-IR, NMR, absorption and photoluminescence spectroscopy to study the physical and optoelectronic properties.

2. Experimental

2.1 Materials and methods used

All reagents like hexane, ethanol and 25% NH_4OH, used in the synthesis of complexes **D1–D4** were analytically pure and required no additional purification steps. Furthermore, Sigma-Aldrich was the source for $DyCl_3{\cdot}6H_2O$ (99.9%), 2, 2′-bipyridine (99.5%), 1,10-phenanthroline (99.5%) and 2, 9-dimethyl-1,10-phenanthroline (99.5%), while 2,9-dibromo-1,10-phenanthroline (96%) was purchased from BLDpharm. The ligand BBA was synthesized by following the literature procedure outlined in ref. 22. A PerkinElmer 2400 Analyzer was utilized to perform elemental analysis. Molar conductivity measurements of the complexes were carried out using a MICROSIL bridge-type conductivity bridge in 10^{-3} M dimethyl

sulfoxide solution at 25 ± 1 °C. The thermal behaviour of the complexes was studied *via* STA-7300 by Hitachi at 10 °C per minute under an inert atmosphere. The complexes were also characterised by FT-IR spectroscopy with the help of a PerkinElmer 5700 spectrometer. Thin KBr pellets of the complexes were formed and recorded over a range of 4000–400 cm^{-1}. Proton NMR spectroscopy was performed on a Bruker Avance II 400 NMR spectrometer, using $CDCl_3$ as the solvent. A Potentiostat-4000 was operated at a speed of 0.1 V s^{-1} for carrying out the cyclic voltammetric (CV) study. The electronic spectra were captured in dichloromethane (DCM) by employing a Shimadzu 2450 spectrophotometer. Optical properties of the solid complexes were studied using a Horiba Jobin YVON Fluorolog FL-3-11 spectrophotometer having a slit width of 5 nm. The lifetimes of the complexes were measured with an F-7000 FL Spectrophotometer. All analyses were carried out at room temperature, unless otherwise specified.

2.2 Synthesis pathway

The trivalent dysprosium complexes were synthesized using a straightforward method with a molar ratio of 1 : 3 : 1 for $DyCl_3 \cdot 6H_2O$, BBA and ancillary ligands. To begin, an ethanolic solution of BBA (6.48 mmol, 1.562 g) was prepared and then NH_4OH (25%) was added to it dropwise. The mixture was left at rest until the ammonia fumes were no longer perceptible, indicating the formation of the ammonium salt of the diketone. Next, ethanolic dysprosium chloride hexahydrate ($DyCl_3 \cdot 6H_2O$; 2.16 mmol, 0.814 g) and the respective ancillary ligand (2.16 mmol) (bpy: 0.337 g; phen: 0.389 g; brphen: 0.730 gm; neo: 0.449 g) solutions were introduced to the ammoniated salt solution. To maintain a slightly basic environment (pH 6–7), additional ammonium hydroxide was added as needed. The prepared mixture was stirred continuously overnight to ensure thorough complexation. After stirring, the solution was kept undisturbed to facilitate the gradual evaporation of ethanol, resulting in the formation of a solid product. The precipitates were then washed several times, first with ethanol to remove any residual reagents and subsequently with hexane to further purify the solid. The synthetic approach used for preparing the **D1–D4** complexes is illustrated in Fig. 2.[23–25]

D1: Color: wheatish white. Molecular weight: 1039. Yield: 79%. Molar conductance (Ω^{-1} cm^2 mol^{-1}): 12.96. Elemental composition of $C_{40}H_{32}Br_3N_2O_6Dy$, calculated (%): C, 46.24; H, 3.10; N, 2.70 and experimental (%): C, 46.29; H, 3.17; N, 2.64. FT-IR stretching frequencies (cm^{-1}): 2922 (ν_{CH_3}); 1591 ($\nu_{C=O}$); 1559 ($\nu_{C=N}$); 1514 ($\nu_{C=C}$); 844 (ν_{C-H}); 564 (ν_{Dy-N}); 465 (ν_{Dy-O}). ^{1}H NMR (δ-ppm): −10.12 (2H bpy); −50.12 (2H bpy); −64.35 (2H bpy); −69.42 (2H bpy); 10.45 (6H BBA); 11.89 (9H BBA); 16.71 (6H BBA); 147.10 (3H BBA).

D2: Color; wheatish white. Molecular weight: 1063. Yield: 77%. Molar conductance (Ω^{-1} cm^2 mol^{-1}): 11.61. Elemental composition of $C_{42}H_{32}Br_3N_2O_6Dy$, calculated (%): C, 47.46; H, 3.03; N, 2.64 and experimental (%): C, 47.51; H, 3.05; N, 2.58. FT-IR stretching frequencies (cm^{-1}): 2921 (ν_{CH_3}); 1590 ($\nu_{C=O}$); 1558 ($\nu_{C=N}$); 1513 ($\nu_{C=C}$); 842 (ν_{C-H}); 562 (ν_{Dy-N}); 465 (ν_{Dy-O}). ^{1}H NMR (δ-ppm): −11.59 (2H phen); −57.45 (2H phen); −64.78 (2H phen); −70.81 (2H phen); 10.37 (6H BBA); 12.92 (9H BBA); 16.42 (6H BBA); 150.14 (3H BBA).

D3: Color: creamish white. Molecular weight: 1221. Yield: 74%. Molar conductance (Ω^{-1} cm^2 mol^{-1}): 12.02. Elemental composition of $C_{42}H_{30}Br_5N_2O_6Dy$, calculated (%): C, 41.32; H, 2.48; N, 2.29 and experimental (%): C, 41.27; H, 2.53; N, 2.32. FT-IR stretching frequencies (cm^{-1}): 2923 (ν_{CH_3}); 1593 ($\nu_{C=O}$); 1558 ($\nu_{C=N}$); 1515 ($\nu_{C=C}$); 843 (ν_{C-H}); 563 (ν_{Dy-N}); 467 (ν_{Dy-O}). ^{1}H NMR (δ-ppm): −56.19 (2H brphen); −70.26 (2H brphen); −74.62 (2H brphen); 10.52 (6H BBA); 12.94 (9H BBA); 16.89 (6H BBA); 153.61 (3H BBA).

D4: Color: wheatish white. Molecular weight: 1091. Yield: 73%. Molar conductance (Ω^{-1} cm^2 mol^{-1}): 10.74. Elemental composition of $C_{44}H_{36}Br_3N_2O_6Dy$, calculated (%): C, 48.44; H,

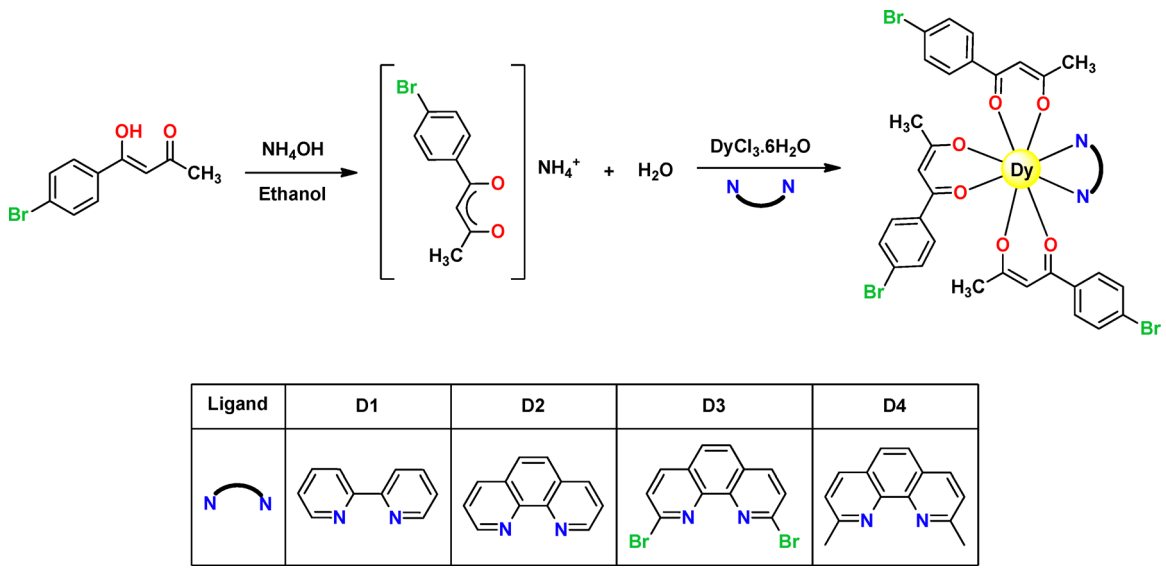

Fig. 2 Synthetic route for the **D1–D4** complexes with various neutral ligands.

3.33; N, 2.57 and experimental (%): C, 48.41; H, 3.37; N, 2.62. FT-IR stretching frequencies (cm^{-1}): 2922 (ν_{CH_3}); 1589 ($\nu_{C=O}$); 1557 ($\nu_{C=N}$); 1513 ($\nu_{C=C}$); 844 (ν_{C-H}); 563 (ν_{Dy-N}); 466 (ν_{Dy-O}). ^{1}H NMR (δ-ppm): −10.72 (6H neo); −55.43 (2H neo); −62.54 (2H neo); −68.09 (2H neo); 10.64 (6H BBA); 12.02 (9H BBA); 16.76 (6H BBA); 152.23 (3H BBA).

3. Findings and interpretation

3.1 Preliminary analysis

Elemental analysis was used to determine the carbon, hydrogen and nitrogen percentage compositions of the synthesized complexes. A close agreement between the observed and calculated values of the complexes affirmed the formation of the complexes in the correct stoichiometry. The low molar conductivity values of the complexes confirm their non-electrolytic nature. The dysprosium complexes exhibited good solubility in DCM and DMSO and were observed to be fairly stable at ambient temperature and pressure.

3.2 Thermogravimetric analysis

The thermal behaviour of the complexes **D1–D4** was studied under a controlled heating rate and the corresponding TG curves are shown in Fig. 3. All three complexes remained stable up to ∼200 °C, confirming their anhydrous nature and the absence of lattice or coordinated water molecules. Thereafter, a distinct two-step decomposition process was observed. Complex **D1** decomposed in the range of 240–560 °C with an experimental weight loss of 84.64% (calculated 82.77%), while **D2** decomposed between 219 and 571 °C showing a weight loss of 84.99% (calculated 83.19%). Similarly, **D3** exhibited decomposition from 204–542 °C with a total mass loss of 86.93% (calculated 84.95%). The decomposition process leaves behind a stable oxide residue, consistent with Dy_2O_3 as the final product.

Complex **D4** also exhibited anhydrous behaviour, with no weight loss up to 215 °C, followed by a two-step decomposition process ranging from 215 °C to 613 °C. The first stage accounted for 62.39% weight loss, close to the theoretical value of 66.29% for the loss of three diketonic moieties, while the second step contributed 21.27% (theoretical 19.08%) corresponding to the dissociation of the ancillary ligand. The overall experimental weight loss was 85.38% (calculated 83.66%), again leaving behind Dy_2O_3 as the final decomposition residue. The relatively high onset of decomposition across all four complexes highlights their excellent thermal stability, which

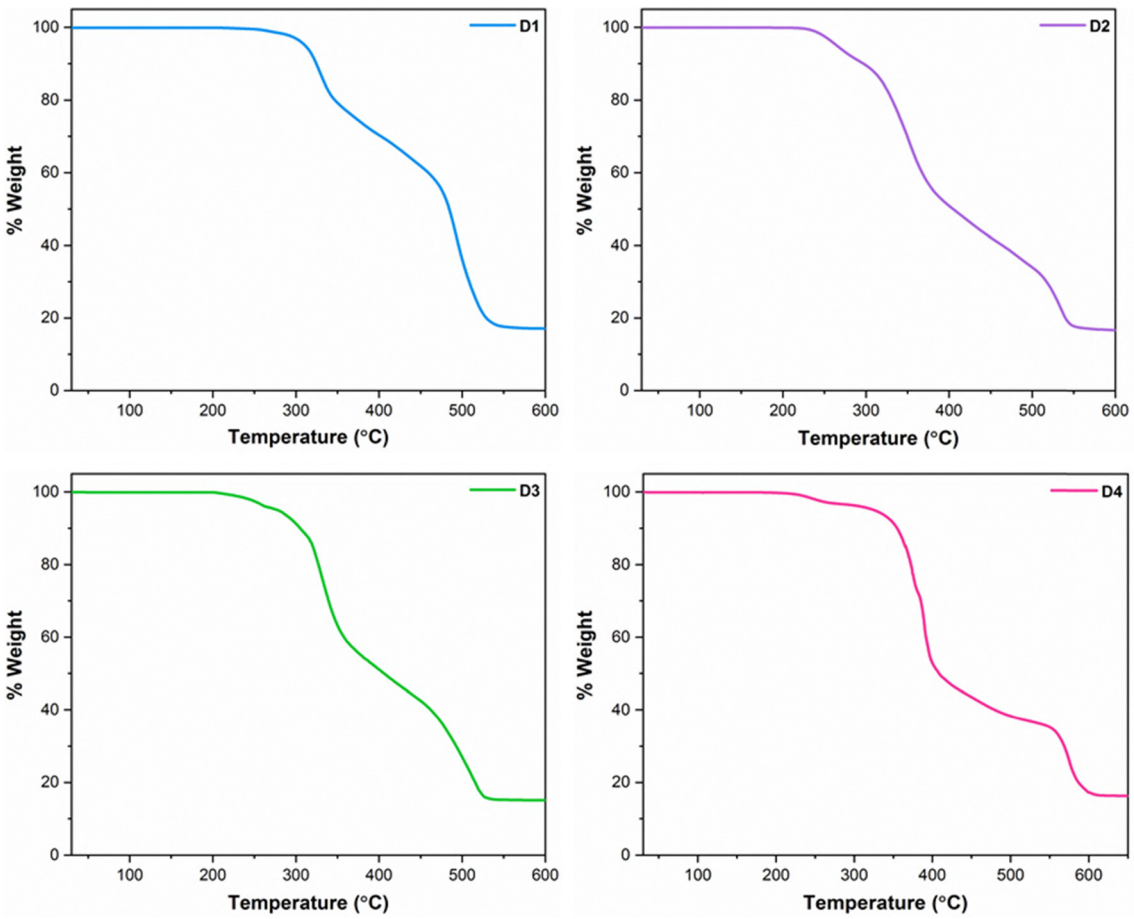

Fig. 3 Thermogravimetric profile of **D4**.

is favourable for potential applications in optoelectronic devices, particularly as OLED emissive layer materials where robust stability at elevated temperatures is essential.[26]

3.3 FT-IR spectral investigation

A detailed investigation of the infrared spectra of the complexes was carried out. The broad FT-IR band at around 3456–3440 cm^{-1} in the spectrum of the uncoordinated BBA ligand assigned to ν_{OH} modes, disappeared in the spectra of the complexes. This confirmed the complexation of Dy(III) ions with the diketonic moiety. Strong FT-IR bands at 1604 cm^{-1} and 1507 cm^{-1} respective to $\nu_{C=O}$ and $\nu_{enolic\ C=C}$ stretching oscillatory modes of free β-diketone appear at approximately 1593–1588 cm^{-1} in the spectrum of the complexes.[27] Strong peaks corresponding to $\nu_{C=C}$ and ν_{CH_3} were also observed at 1479 cm^{-1} and 2922 cm^{-1} in the complexes. The $\nu_{C=N}$ stretching bands at 1578 cm^{-1} (bpy),[28] 1591 cm^{-1} (phen)[29] and 1593 cm^{-1} (neo)[30] in uncoordinated ligands shifted to lower wavenumbers (~1559–1552 cm^{-1}) in the complexes further confirming the bonding with these ligands in the respective complexes. The bonding of the trivalent dysprosium ion with nitrogen and oxygen atoms of the corresponding ancillary and BBA units is confirmed by the presence of ν_{Dy-N} and ν_{Dy-O} stretching frequency at 562 cm^{-1} and 465 cm^{-1}, respectively.[31,32] FT-IR spectral analysis revealed the absence of a characteristic broad O–H stretching peak at ~3300 cm^{-1}, which aligns with thermal analysis results and confirms the anhydrous state of the complexes.

3.4 Proton NMR studies

The chemical shift values (in ppm) for paramagnetic **D1–D4** complexes along with uncoordinated β-diketone were recorded in $CDCl_3$. All the complexes exhibit paramagnetic shifts, which are dipolar in nature originating from magnetic anisotropy of the Dy(III) ion. The free BBA ligand exhibits peaks at 15.95 (–OH); 6.09 (–CH); 7.5, 7.59, 7.70, 7.82 (–CH aromatic); and 2.28 ($-CH_3$). At room temperature, paramagnetic shifts of protons in the β-diketone moiety were in stark contrast to those of the protons of ancillary ligands, exhibiting upfield and downfield shifts, respectively.[33,34] The disappearance of the enolic OH signal in the spectra of the complexes is a clear indication of the Dy(III) ion's coordination to the oxygen atom of the BBA ligand.

3.5 Electronic absorption spectral analysis

Fig. 4 presents the electronic spectra of the free BBA ligand and **D1–D4** complexes in 10^{-5} mol L^{-1} DCM solution. At 299 nm, the electronic spectral profile of BBA exhibits a broad band corresponding to π–π* transitions. However, the complexes exhibited broad bands, featuring two maxima with different intensities. The maxima in the electronic spectral profiles of the complexes owing to π–π* transitions were recorded at 319 nm for **D1**, 324 nm for **D2**, 333 nm for **D3** and 345 nm for **D4**. A bathochromic shift was observed in complexes **D1** through **D4** relative to the free BBA ligand. This shift is likely due to the enhanced π-electron conjugation and stabilization of the chromophoric ligand orbitals upon coordination to the metal ion.[35]

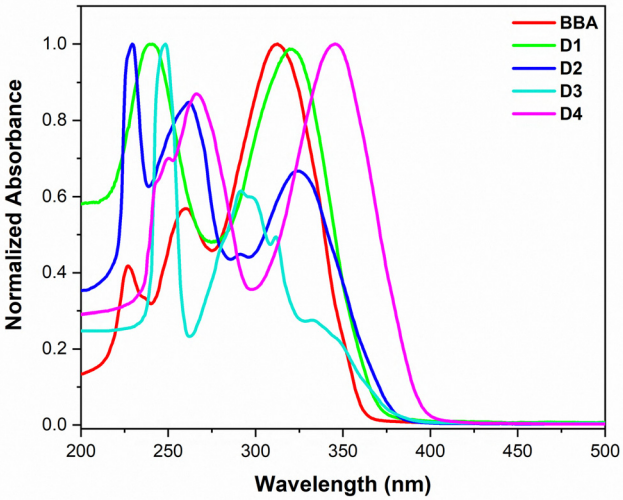

Fig. 4 Normalized absorption profiles of BBA and **D1–D4** in DCM.

3.6 Band gap analysis

Band gap (E_g) signifies the difference in energy between the valence and conduction band in the complexes. Determining this energy gap is vital for evaluating the potential application of any material, particularly optoelectronic applications. Applying Tauc's relation (eqn (1)), which relates absorption coefficient (α) to the band gap (E_g), the Tauc plot for **D1–D4** (Fig. 5) was constructed.[36,37]

$$(\alpha h\nu)^2 = A(h\nu - E_g)^n \quad (1)$$

where $h\nu$ is the photon energy, n is the power dependence of the electronic transition and α is the absorption coefficient.

The energy gaps of the complexes were determined by the point of intersection of the extended linear segment of the graph to the photon energy axis. The Tauc plot was constructed considering the absorption edge at higher wavelength. Table 2 and Fig. 5 enlist the band gap of the complexes determined from their electronic spectra. With energy gaps comparable to those of semiconductors (2–4 eV), these complexes can be utilized as semiconducting materials.[38]

3.7 Cyclic voltammetry

Cyclic voltammetric experiments were conducted on the complexes **D1** and **D4** in a 0.001 M DCM solution, using tetrabutylammonium perchlorate as the supporting electrolyte, as shown in Fig. 6. A three-electrode electrochemical cell was constructed using a vitreous carbon working electrode, a platinum wire counter electrode and a silver/silver chloride reference electrode. The energies of the frontier molecular orbitals were calculated from the redox potentials obtained from the current *vs.* potential plot, using eqn (2) and (3).[39,40]

$$E_{HOMO} = -[(E_{ox} - E_{1/2(ferrocene)}) + 4.8]\ eV \quad (2)$$

$$E_{LUMO} = -[(E_{red} - E_{1/2(ferrocene)}) + 4.8]\ eV \quad (3)$$

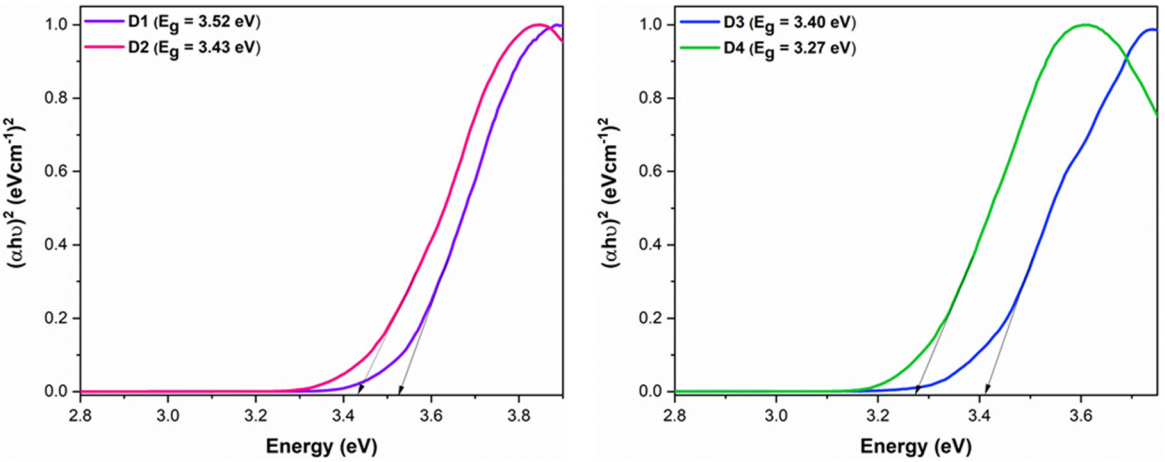

Fig. 5 Optical band gap determination of **D1–D4** using Tauc plots.

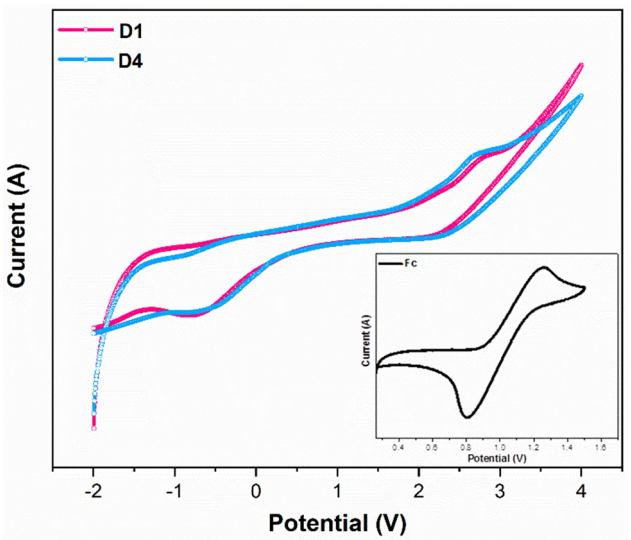

Fig. 6 Cyclic voltammograms of **D1** and **D4**, with the Ferrocene profile in the inset.

The half potential of Ferrocene, which was used as an internal standard determined from the *I–V* graph (inset of Fig. 6), was 1.03 V. Table 1 enlists the obtained electrochemical data. The electronic band gap (E_g^e) estimated from the frontier molecular orbitals agrees with the optical band gap (E_g).

3.8 Photoluminescence properties

3.8.1 Excitation spectra. Photoluminescence excitation properties of solid **D1–D4** complexes were assessed by exciting them at 480 nm ($^4F_{9/2} \rightarrow {}^6H_{15/2}$ transitions) and 575 nm ($^4F_{9/2} \rightarrow {}^6H_{13/2}$ transitions). However, a comparatively stronger excitation was observed at 575 nm than at 480 nm. All the complexes exhibited a broad and intense spectral band (Fig. 7) corresponding to chromophoric moieties between 214 nm and 530 nm, showing two λ_{max} of differing intensities. The higher-intensity maximum at a longer wavelength was used to excite the complexes for emission spectral analysis.

3.8.2 Emission spectra. The wavelength used for excitation (λ_{ex}), along with the difference of energy between the ligand's triplet level and the lanthanide ion's resonance level has an important role in influencing the emission characteristics of the metal complexes. Proper selection of the incident wavelength used for excitation enhances the relative emission intensity of the complex. Fig. 8 displays the PL emission profiles of solid **D1–D4**, recorded upon excitation at their respective λ_{ex} values as determined from the excitation spectra. The emission profiles of **D1–D4**, resulting from the depopulation of the $^4F_{9/2}$ energy level, showed three distinct peaks within

Table 1 Comparative analysis of the redox potential and E_g^e for **D1** and **D4**

Complex	$E_{ox.}$ (V)	$E_{red.}$ (V)	E_{HOMO} (eV)	E_{LUMO} (eV)	E_g^e (eV)
D1	2.77	0.79	6.54	2.98	3.56
D4	2.68	0.62	6.45	3.15	3.30

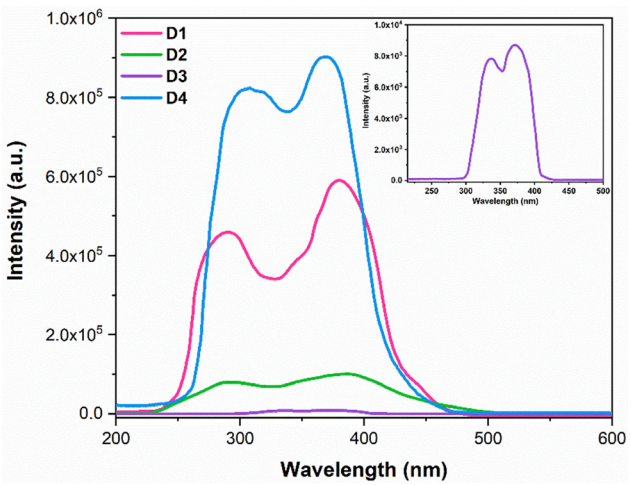

Fig. 7 Solid-state excitation spectra of the **D1–D4** complexes.

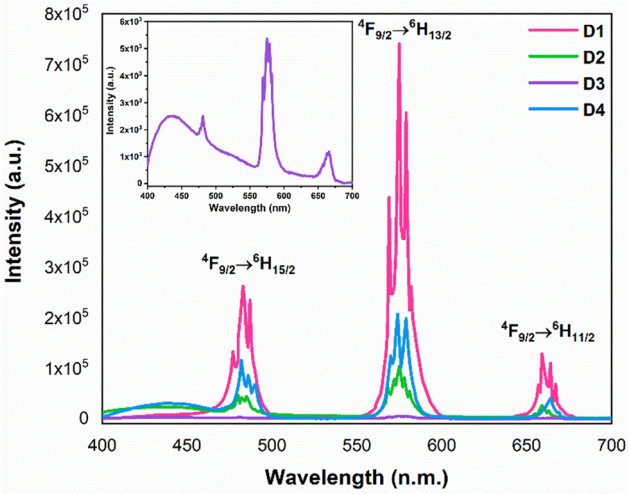

Fig. 8 Solid state emission spectra of the **D1–D4** complexes.

the wavelength range of 450 to 680 nm. There was no substantial difference in the emission peak positions of the ternary Dy(III) complexes. The shortest wavelength peak was located at ~480 nm and corresponded to the magnetic dipole transition between the $^4F_{9/2}$ and $^6H_{15/2}$ energy levels. This transition is also referred to as the blue line (B).[41] A second peak, appearing at 575 nm, was attributed to the induced electric dipole transition between the $^4F_{9/2}$ and $^6H_{13/2}$ levels and is commonly known as the yellow line (Y). This peak dominated the emission spectrum of the complexes. The remaining peak at ~665 nm, representing the $^4F_{9/2}$ to $^6H_{11/2}$ transition, displayed the lowest intensity.[42] Alongside the characteristic Dy(III) emission peaks, **D2**, **D3** and **D4** exhibited a broad band, which is assigned to ligand-centered emission. This band spanned the region of 400–450 nm.

The intensified yellow emission relative to the blue line indicates that the Dy(III) ion likely resides in an environment of low molecular symmetry or within a complex lacking an inversion center. The blue emission line is magnetically permitted and is unaffected by the local magnetic field surrounding the Dy(III) ion, but the presence of stark splitting in the $^4F_{9/2}$ → $^6H_{15/2}$ transition suggests a more asymmetrical environment for the Dy(III) ion.[43] In contrast, the spectra of [Dy(hfpd)$_3$phen],[44] highlights the influence of ligand symmetry on the electronic environment of the Dy(III) ion. Among the synthesized Dy(III) complexes, **D1** exhibited the highest emission intensity while **D3** displayed the weakest, with **D4** and **D2** in between. This variation in luminescence intensity can be attributed to the different neutral ligands, which alter the coordination environment around the Dy(III) ion. The structure of these ligands, particularly their rigidity, plays a crucial role in determining the luminescence properties. Specifically, better energy level matching and smaller steric effects among the ancillary ligands and the diketone ligand contributes to enhanced emission intensity, explaining the observed trend, which is discussed further in Section 3.11. Table 2 details the excitation (λ_{ex}) along with the emission wavelengths (λ_{em}).

Table 2 Photophysical parameters for **D1–D4**

Complex	λ_{abs}^{max}	E_g (eV)	λ_{ex} (nm)	λ_{em} (nm)
D1	240, 319	3.52	289, 379	483, 575, 659
D2	261, 324	3.43	307, 368	480, 575, 659
D3	248, 295, 333	3.40	337, 370	481, 575, 666
D4	266, 345	3.27	291, 385	482, 574, 664

3.8.3 Branching ratio. A luminescence branching ratio (β) is commonly used to quantify the distribution of luminescence intensity among the spectral bands and is expressed as the ratio of the radiative transition rate for a given transition to the total of the radiative transition rates of all other transitions. In simpler terms, it shows the relative intensity of each transition. In Table 3, the percentage values of β, calculated from the integration of the emission spectra using eqn (4) are tabulated.[45,46]

$$\beta = \frac{A_{\psi J-\psi' J}}{\sum A_{\psi J-\psi' J}} \times 100 \quad (4)$$

Here, $A_{\psi J-\psi' J}$ corresponds to the total area of the observed photoluminescence emission peak. The highest value of β for solid **D1–D4** corresponds to the $^4F_{9/2}$ → $^6H_{13/2}$ transition with $^6H_{15/2}$ next in line and thereafter the $^6H_{11/2}$ transition. The branching ratio serves as a key parameter in laser design, indicating the likelihood of stimulated emission occurring from a particular transition. A predominance of ΔJ = 2 transitions, constituting roughly 60% of the aggregate emission in **D1–D4** observed through β ratio analysis suggests its applicability for laser amplification.[47] Intensity ratio, commonly called yellow/blue (Y/B) ratio, refers to the ratio of electric dipole transition to the magnetic dipole transition, helps in understanding uniformity around the Dy(III) ion.[48] The observed Y/B ratio as presented in Table 3 strongly supports the presence of highly asymmetric surroundings in the solid complexes.

3.9 Lifetime analysis

The emission lifetime of the powdered **D1–D4** complexes was investigated for dominant emission transition ($^6H_{13/2}$) of the Dy(III) ion at 574 nm with ~370 nm excitation wavelength. Fig. 9 shows the semilog decay profiles of the solid **D1–D4** complexes. All the experimental decays were best fitted with a single-exponential function corresponding to eqn (5), confirming the presence of a single luminescent centre.[49,50]

$$I = I_0 e^{(-t/\tau)} \quad (5)$$

Table 3 Branching ratio of the characteristic peaks, intensity ratios and lifetime of **D1–D4**

	Branching ratio				
Complex	ΔJ = 3	ΔJ = 2	ΔJ = 1	Intensity ratio	Lifetime (μs)
D1	27.00	62.92	10.06	2.33	3.59 ± 0.025
D2	30.24	61.00	8.75	2.01	3.10 ± 0.033
D3	22.87	65.29	11.83	2.85	2.36 ± 0.004
D4	32.36	60.30	7.32	1.86	3.38 ± 0.011

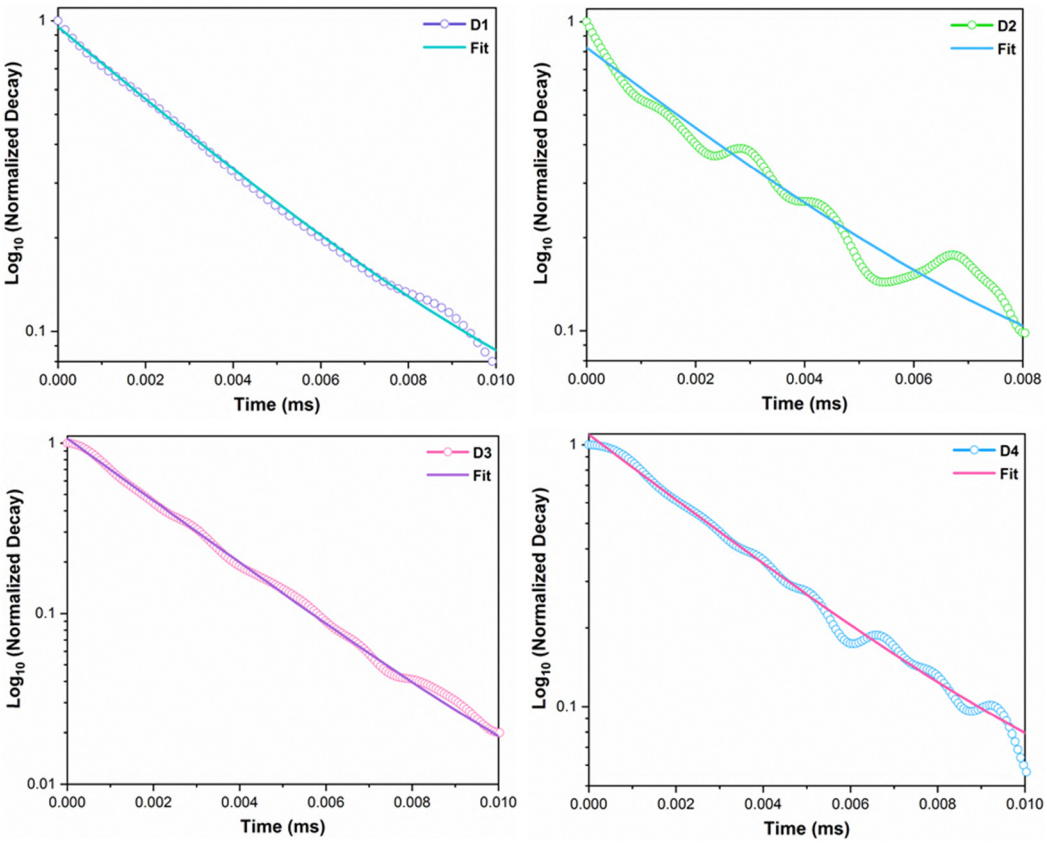

Fig. 9 Semilog decay profiles of **D1–D4**.

Here, the exponential decay of intensity I over time t is represented with τ indicating the characteristic decay time and I_0 depicting the initial intensity. Table 3 details the luminescence lifetimes of the synthesized Dy(III) complexes ranging from 2.36 to 3.59 μs, with **D1** exhibiting the highest value.

These lifetimes are comparable to and in some cases exceed, those reported for related ternary Dy(III) complexes, such as $Dy(tfa)_3(bpy)$ (2.87 μs), $Dy(tfa)_3(phen)$ (2.89 μs), $Dy(tfa)_3(H_2O)_2(Me_2CO)$ (2.50 μs) and $[Dy(acac)_3(5\text{-Br-}2,2'\text{-bpy})]$ (3.20 μs).[51,52] The slightly higher lifetime values observed for **D1–D4** can be attributed to several structural factors. First, the lack of coordinated water molecules in the present complexes reduces non-radiative deactivation *via* high-energy O–H vibrations, which is a known quenching pathway in aqua-containing complexes such as $Dy(tfa)_3(H_2O)_2(Me_2CO)$. Second, all four complexes incorporate *N*,*N*′-donor neutral ligands, which replace potentially labile solvent molecules and provide a more rigid coordination environment, effectively minimizing vibrational relaxation. Furthermore, although the diketonate ligand BBA used in these complexes bears a $-CH_3$ group, which could allow some vibrational quenching, the presence of extended aromatic systems, particularly phenyl rings, in both BBA and the neutral ligands appears to enhance rigidity and suppress non-radiative energy loss. This may explain why the lifetimes of **D1–D4** are still relatively high. In contrast, the comparatively shorter lifetimes observed for the present BBA-based complexes, relative to $[Dy(bfa)_3(phen)]$ (0.77 ms),[53] can be attributed to the presence of $-CH_3$ groups in BBA, which are less effective in suppressing non-radiative decay than the strongly electron-withdrawing $-CF_3$ groups in bfa. Thus, the enhanced lifetimes observed in **D1–D4** reflect an optimized balance of ligand design, absence of quenching solvent molecules and structural rigidity imparted by aromatic substituents.

3.10 Chromaticity parameters

The color characteristics of the complexes were evaluated by calculating the (x, y) coordinates and (u', v') coordinates using the PL emission data, and the quality of white light produced from the Dy(III) complexes was examined through CCT values. The CIE 1931 chromaticity coordinates (x, y) were obtained directly using the emission intensity distribution and other parameters were subsequently computed using these coordinates *via* eqn (6) and (7).[54–56]

$$u' = \frac{4x}{-2x + 12y + 3}, \quad v' = \frac{9y}{-2x + 12y + 3} \tag{6}$$

$$\mathrm{CCT} = -437n^3 + 3601n^2 - 6861n + 5514.31 \tag{7}$$

The reciprocal slope n, as defined in eqn (7), is determined by the formula $n = (x - x_e)/(y - y_e)$,[57] where x_e and y_e correspond to color epicentres with values of 0.332 and 0.186,

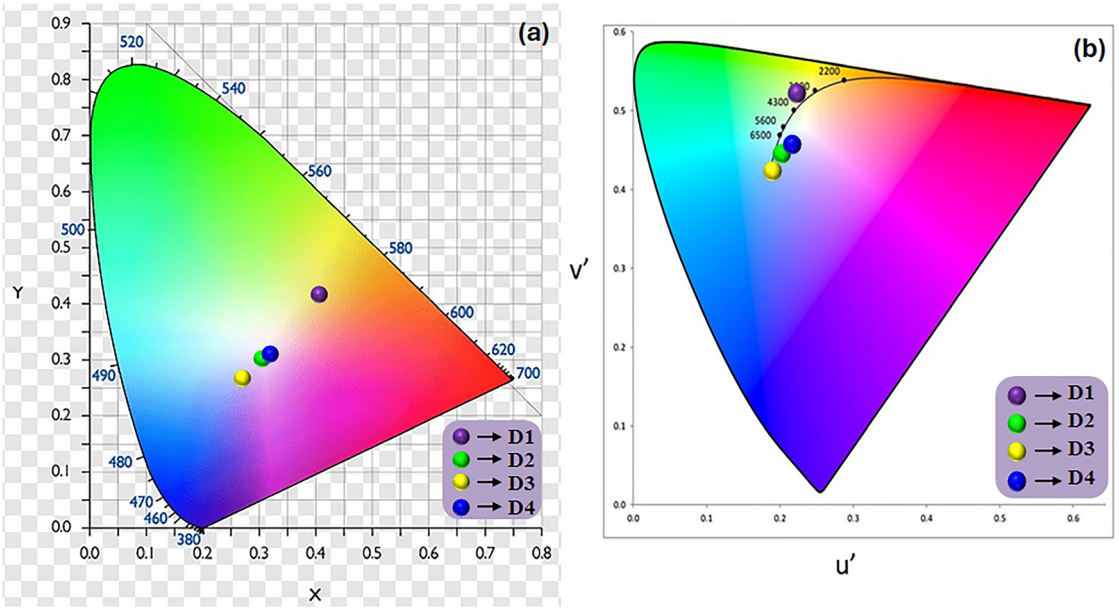

Fig. 10 CIE color coordinate plots for **D1–D4** complexes: (a) *x*, *y* and (b) *u*′, *v*′.

respectively. Correlated color temperature (CCT) is a standard metric used to assess a light source's quality by relating its color appearance to that of an ideal blackbody radiator at a given temperature in Kelvin. A lower CCT value indicates a warmer light, while a higher CCT value suggests a cooler light. Specifically, CCT values below 3200 K are typically considered warm, while those above 4000 K are classified as cool. CCT values above 3200 K for the solid-state Dy(III) complexes suggest that they emit cool-toned light.[58] Fig. 10 displays the *x*, *y* and *u*′, *v*′ coordinates of the complexes.

Variation in emission color among the Dy(III) complexes, as influenced by the neutral ligands, is evident from the CIE chromaticity diagram. Complex **D1** falls within the yellow region, consistent with the dominance of a yellow emission band. Complexes **D2** and **D4** are located near the white region of the CIE triangle, attributed to the appropriate balancing of the intensities of the blue and yellow emission bands. In contrast, **D3** lies in the blue region, due to a prominent blue ligand-centered band in its emission spectra. The calculated values of the color coordinates of **D2** and **D4** were found to match the white coordinates of both the National Television System Committee (NTSC) (0.310, 0.316) and commercial LEDs (0.32, 0.32).[59] The color purity of the synthesized complexes was also quantified using eqn (8), where the coordinates of white light and dominant wavelength are represented by (x_i, y_i) and (x_d, y_d), correspondingly.[60,61]

$$\mathrm{CP} = \sqrt{\frac{(x-x_i)^2+(y-y_i)^2}{(x_d-x_i)^2+(y_d-y_i)^2}} \times 100\% \qquad (8)$$

A complete listing of all the color parameters is provided in Table 4. Among the studied complexes, **D4** displayed the minimum color purity (9.80%) and reflects its superior approximation to pure white light.

3.11 Energy transfer mechanism

The luminescence of trivalent dysprosium complexes primarily depends on the efficiency of transfer of energy from coordinated moieties to the Dy(III) centre. Since direct excitation of Ln^{3+} ions is inefficient because of the parity-forbidden nature of the 4f–4f transitions, an indirect sensitization pathway *via* ligand-to-metal energy transfer is required. Primary ligand, BBA and the neutral ligands (bpy, phen, brphen and neo) chosen in this study play a crucial role in this process by acting as organic antenna chromophores. The proposed mechanism for indirect excitation is schematically represented in Fig. 11. Upon photoexcitation, electrons in the ligand are promoted from the singlet ground state (S_0) to the singlet excited state (S_1), followed by intersystem crossing (ISC) to the triplet state (T_1). From the T_1 state, the transfer of energy occurs to emissive states of the metal ion *via* a nonradiative energy transfer mechanism. In the view of Dexter's theory, the efficiency of this transfer of energy depends on the energy gap (ΔE) between the T_1 and resonance excited state of the Dy(III) ion ($^4F_{9/2}$).[62,63] Unlike Eu(III) complexes, where $\Delta E(T_1 \rightarrow {}^5D_0)$ should be greater than 2500 cm^{-1} for effective energy transfer, the Dy(III) ion does not have a well-defined threshold for this process in the literature. However, previous studies suggest that an optimal ΔE ensures minimal energy back-transfer and efficient sensitization. In the case of the Dy(III) ion, the $^4F_{9/2}$ level is typically around 20 833 cm^{-1}.[64] The T_1 state energies of bpy

Table 4 Color characteristics corresponding to **D1** to **D4**

Complex	(*x*, *y*)	(*u*′, *v*′)	CCT	CP (%)
D1	(0.4036, 0.4234)	(0.2219, 0.5239)	3760.60	48.55
D2	(0.3059, 0.3003)	(0.2042, 0.4511)	7273.96	18.20
D3	(0.2798, 0.2780)	(0.1937, 0.4332)	10646.29	32.45
D4	(0.3268, 0.3113)	(0.2149, 0.4607)	5805.28	9.80

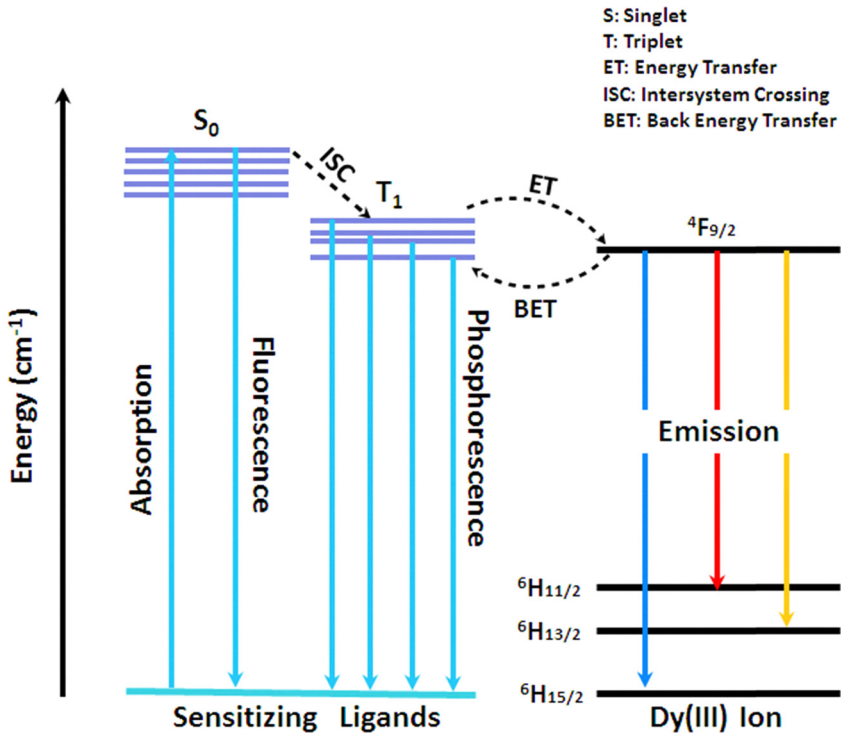

Fig. 11 Sensitization mechanism and emission pathway of Dy(III) in **D1–D4**.

(22 900 cm^{-1}),[65] phen (22 100 cm^{-1}),[66] brphen (21 027 cm^{-1}) and neo (22 624 cm^{-1})[67] vary in their ability to transfer energy to the Dy(III) ion. **D1** (bpy, 22 900 cm^{-1}): large energy gap ($\Delta E \sim 2067$ cm^{-1}) minimizes back-transfer, leading to efficient Dy(III) ion sensitization and the highest observed emission intensity. **D2** (phen, 22 100 cm^{-1}): the moderate gap ($\Delta E \sim 1267$ cm^{-1}) results in effective sensitization, but some ligand-based emission is observed due to partial back-transfer. **D3** (brphen, 21 027 cm^{-1}): the small gap ($\Delta E \sim 194$ cm^{-1}) makes back-transfer significant, reducing the Dy(III) emission intensity and leading to a pronounced ligand-based band. **D4** (neo, estimated 22 624 cm^{-1}): the intermediate gap ($\sim$1791 cm^{-1}) allows some back energy transfer, causing ligand-based emission alongside Dy(III) centred emission.

The observed emission intensity order (**D1** > **D4** > **D2** > **D3**) is consistent with this energy transfer model, where bpy (**D1**) provides the most efficient sensitization and brphen (**D3**) exhibits the highest back-transfer. The presence of a ligand-based emissive band in **D2**, **D3** and **D4** further confirms back transfer of energy from Dy(III) to the ancillary moiety in these complexes. Notably, the overall low-energy nature of these complexes can be attributed to the common ligand BBA, whose triplet state energy (21 325 cm^{-1}) lies in close proximity to the emissive $^4F_{9/2}$ level of the Dy(III) ion, thereby facilitating both forward and reverse energy transfer processes.

4. Conclusions

In this study, a series of ternary dysprosium complexes, denoted by the general formula [Dy(BBA)$_3$L] (where L = bpy, phen, brphen, neo), were synthesized. Spectroscopic analyses confirmed coordination of Dy(III) through oxygen atoms of the β-diketone and nitrogen atoms of the neutral ligands. All the complexes exhibited excellent thermal stability (decomposition above 200 °C), validating their structural robustness for optoelectronic applications. The specific impact of substituents on the luminescent behavior of the metal complexes has been determined. The emission color can be adjusted by structural modification of the coordinating ligand. The chromaticity coordinates of the complexes were situated in the white, yellow and blue regions of the color triangle. Specifically, the white light emission observed in complexes **D2** and **D4**, characterized by a CCT value exceeding 3200 K (placing them in the cool white region), likely results from a balanced intensity between the yellow and blue emission bands of dysprosium complexes. This white light emission from the solid Dy(III) powder holds potential for applications in white light-emitting devices (WLEDs). The high branching ratios (above 60%) across all complexes suggest their potential utility in laser systems. In addition to their structural robustness and tunable luminescent profiles, the Dy(BBA)$_3$L complexes demonstrate semiconducting properties, as observed by close agreement among the optical and electrochemical energy gaps. Upon excitation at 575 nm, visible emission typical of Dy(III) ions was observed, with particularly strong yellow-white luminescence in **D2** and **D4**. The clear splitting of the $^4F_{9/2} \rightarrow {}^6H_{13/2}$ transition underscores the asymmetric ligand field, influenced by the nature of the coordinating neutral ligand. The energy transfer mechanism confirms the sensitization role of the organic moiety, with **D3** exhibiting the weakest emission, presumably due to its

lower triplet energy level of the neutral ligand. These photophysical insights further affirm the suitability of these complexes for optoelectronic applications, including WLEDs and potential laser media.

Author contributions

Sofia Malik: data curation and writing – original draft; Komal Jakhar and Devender Singh: writing – review and editing and supervision; Swati Dalal: methodology; Vandana Aggarwal: formal analysis; Sumit Kumar: visualization and investigation; Parvin Kumar: validation; Parvin Kumar: software.

Conflicts of interest

The authors declare that they have no known competing financial interests or personal relationships that could have appeared to influence the work reported in this paper.

Data availability

The authors affirm that the information/data of this research article is available inside the article.

Acknowledgements

Sofia Malik is thankful to UGC-New Delhi for providing the JRF [221610212505].

References

1 J. Corredoira-Vázquez, C. González-Barreira, A. M. García-Deibe, J. Sanmartín-Matalobos, M. A. Hernández-Rodríguez, C. D. Brites, L. D. Carlos and M. Fondo, *Inorg. Chem. Front.*, 2024, **11**, 1087–1098.
2 D. Singh and S. Sheoran, *J. Mater. Sci.:Mater. Electron.*, 2016, **27**, 12707–12718.
3 D. Singh, V. Tanwar, A. P. Simantilleke, B. Mari, P. S. Kadyan and J. Singh, *J. Mater. Sci.:Mater. Electron.*, 2016, **27**, 2260–2266.
4 T. Xian, Q. Meng, F. Gao, M. Hu and X. Wang, *Coord. Chem. Rev.*, 2023, **474**, 214866.
5 A. De Almeida, B. Santos, B. Paolo and M. Quicheron, *Renewable Sustainable Energy Rev.*, 2014, **34**, 30–48.
6 G. He, D. Guo, C. He, X. Zhang, X. Zhao and C. Duan, *Angew. Chem. Int. Ed.*, 2009, **48**, 6132–6135.
7 S. SeethaLekshmi, A. R. Ramya, M. L. P. Reddy and S. Varughese, *J. Photochem. Photobiol., C*, 2017, **33**, 109–131.
8 D. Singh, S. Bhagwan, R. K. Saini, V. Nishal and I. Singh, Adv Magn, *Opt. Mater.*, 2016, **32**, 473–519.
9 A. Dalal, K. Nehra, A. Hooda, S. Bhagwan, R. K. Saini, D. Singh and S. Kumar, *Inorg. Chem. Commun.*, 2022, **141**, 109620.
10 D. Singh, S. Bhagwan, A. Dalal, K. Nehra, R. K. Saini, K. Singh, A. P. Simantilleke, S. Kumar and I. Singh, *Rare Met.*, 2021, **40**, 2873–2881.
11 K. Nehra, A. Dalal, A. Hooda, S. Bhagwan, R. K. Saini, B. Mari, S. Kumar and D. Singh, *J. Mol. Struct.*, 2022, **1249**, 131531.
12 P. Tao, X. Lü, G. Zhou and W. Y. Wong, *Acc. Mater. Res.*, 2022, **3**, 830–842.
13 D. Singh, S. Bhagwan, A. Dalal, K. Nehra, R. K. Saini, K. Singh, S. Kumar and I. Singh, *J. Lumin.*, 2020, **223**, 117255.
14 A. Dalal, K. Nehra, A. Hooda, D. Singh, P. Kumar, S. Kumar, R. S. Malik and B. Rathi, *Inorg. Chim. Acta*, 2023, **550**, 121406.
15 D. Dragancea, T. Mocanu, D. Avram, M. Răducă, C. Tiseanu and M. Andruh, *Polyhedron*, 2024, **252**, 116886.
16 M. L. P. Reddy and K. S. Bejoymohandas, *Dalton Trans.*, 2025, **54**, 9441–9452.
17 A. Hooda, D. Singh, A. Dalal, S. Malik, S. Redhu, K. Jakhar, S. Kumar, R. S. Malik and P. Kumar, *Inorg. Chem. Commun.*, 2023, **155**, 111018.
18 M. Shang, C. Li and J. Lin, *Chem. Soc. Rev.*, 2014, **43**, 1372–1386.
19 V. Aggarwal, D. Singh, A. Hooda, S. Malik, S. Dalal, S. Redhu, S. Kumar, R. S. Malik and P. Kumar, *J. Lumin.*, 2024, **270**, 120555.
20 V. Aggarwal, D. Singh, K. Nehra, S. Dalal, S. Redhu, P. Kumar, S. Kumar and R. S. Malik, *Mater. Sci. Semicond. Process.*, 2025, **192**, 109427.
21 M. Travadi, R. N. Jadeja and R. J. Butcher, *Polyhedron*, 2024, **247**, 116701.
22 S. Dilli and K. Robard, *J. Chromatogr. A*, 1984, **312**, 109–120.
23 A. Hooda, A. Dalal, K. Nehra, P. Kumar, D. Singh, S. Kumar, R. S. Malik, R. Kumar and P. Kumar, *Luminescence*, 2022, **37**, 1921–1931.
24 A. Hooda, D. Singh, A. Dalal, K. Nehra, S. Kumar, R. S. Malik, R. Kumar and P. Kumar, *J. Photochem. Photobiol., A*, 2023, **440**, 114646.
25 L. Armelao, S. Quici, F. Barigelletti, G. Accorsi, G. Bottaro, M. Cavazzini and E. Tondello, *Coord. Chem. Rev.*, 2010, **254**, 487–505.
26 S. Redhu, D. Singh, K. Nehra, S. Dalal, S. Malik, V. Aggarwal, S. Kumar, R. S. Malik, P. Kumar and J. Sindhu, *J. Mol. Struct.*, 2024, **1311**, 138380.
27 M. Lawrence, E. I. Paulraj and P. Rajesh, *Chem. Phys.*, 2023, **6**, 100226.
28 A. E. Salem, S. A. Sadeek and S. F. Mohammed, *Bull. Fac. Sci.*, 2023, **2023**, 151–161.
29 M. Sengar and A. K. Narula, *J. Fluoresc.*, 2019, **29**, 111–120.
30 S. Malik, K. Jakhar, D. Singh, S. Dalal, S. Redhu, S. Kumar, P. Kumar and J. Sindhu, *J. Mol. Struct.*, 2026, **1349**, 143870.
31 S. Malik, K. Jakhar, D. Singh, S. Kumar, R. S. Malik and P. Kumar, *Opt. Mater.*, 2024, **150**, 115257.
32 A. Hooda, K. Nehra, A. Dalal, S. Singh, R. K. Saini, S. Kumar and D. Singh, *J. Mol. Struct.*, 2022, **1260**, 132848.

33 S. Redhu, D. Singh, S. Dalal, S. Malik, V. Aggarwal, A. Hooda, S. Kumar, R. S. Malik and P. Kumar, *Polyhedron*, 2024, **61**, 117146.
34 R. R. Gimaev, A. S. Komlev, A. S. Davydov, B. B. Kovalev and V. I. Zverev, *Crystals*, 2021, **11**, 82.
35 S. Archer and J. A. Weinstein, *Coord. Chem. Rev.*, 2012, **256**, 2530–2561.
36 A. Dalal, K. Nehra, A. Hooda, S. Singh, D. Singh and S. Kumar, *J. Fluoresc.*, 2022, **32**, 1019–1029.
37 A. Hooda, K. Nehra, A. Dalal, S. Singh, S. Bhagwan, K. Jakhar and D. Singh, *J. Mater. Sci.:Mater. Electron.*, 2022, **33**, 11132–11142.
38 C. Suresh, H. Nagabhushana, G. P. Darshan, R. B. Basavaraj, D. Kavyashree, S. C. Sharma, A. Arulmozhi, B. D. Prasad and H. J. A. Yadav, *Arabian J. Chem.*, 2018, **11**, 460–482.
39 S. Malik, K. Jakhar, D. Singh, S. Redhu, V. Aggarwal, S. Kumar, R. S. Malik and P. Kumar, *Inorg. Chem. Commun.*, 2025, **181**, 115231.
40 A. Hooda, K. Nehra, A. Dalal, S. Singh, R. K. Saini, S. Kumar and D. Singh, *Inorg. Chim. Acta*, 2022, **536**, 120881.
41 K. V. Krishnaiah, K. U. Kumar and C. K. Jayasankar, *Mater. Res. Express*, 2013, **3**, 61–70.
42 C. M. Nandanwar and N. S. Kokode, *Phys. Chem. Solid State*, 2022, **23**, 597–603.
43 W. A. Dar, Z. Ahmed and K. Iftikhar, *J. Photochem. Photobiol., A*, 2018, **356**, 502–511.
44 S. Malik, K. Jakhar, D. Singh, A. Hooda, S. Redhu, S. Dalal, V. Aggarwal, S. Kumar, R. S. Malik and P. Kumar, *RSC Adv.*, 2024, **14**, 22642–22655.
45 A. Pereira, G. Conte, A. D. Faceto, L. A. Nunes, W. G. Quirino, C. Legnani, H. Gallardo, M. Cremona, I. H. Bechtold and F. E. Guimarães, *J. Appl. Phys.*, 2019, **126**, 165501.
46 S. Redhu, D. Singh, S. Dalal, S. Malik, V. Aggarwal, A. Hooda, S. Kumar, R. S. Malik and P. Kumar, *Polyhedron*, 2024, **261**, 117146.
47 A. B. Ganaie and K. Iftikhar, *ACS Omega*, 2021, **6**, 21207–21226.
48 S. Malik, K. Jakhar, D. Singh, S. Dalal, A. Hooda, K. Nehra, S. Kumar, R. S. Malik and P. Kumar, *Luminescence*, 2024, **39**, e4810.
49 Z. Ahmed and K. Iftikhar, *Inorg. Chem.*, 2015, **54**, 11209–11225.
50 S. Dalal, D. Singh, A. Dalal, A. Hooda, S. Malik, S. Kumar, R. S. Malik, P. Kumar and J. Sindhu, *J. Mater. Sci.: Mater. Electron.*, 2024, **35**, 632.
51 W. Chu, Q. Sun, X. Yao, P. Yan, G. An and G. Li, *RSC Adv.*, 2015, **5**, 94802–94808.
52 Q. Shi, J. Liu, J. Wang, X. Yang, X. Zhang, S. Li, P. Sun, J. Chen, B. Li and X. Lü, *Inorg. Chem. Commun.*, 2020, **113**, 107814.
53 J. Feng, H. J. Zhang, S. Y. Song, Z. F. Li, L. N. Sun, Y. Xing and X. M. Guo, *J. Lumin.*, 2008, **128**, 1957–1964.
54 K. Nehra, A. Dalal, A. Hooda, R. K. Saini, D. Singh and S. Kumar, *Polyhedron*, 2022, **217**, 115730.
55 S. Singh, A. P. Simantilleke and D. Singh, *Chem. Phys. Lett.*, 2021, **765**, 138300.
56 C. S. McCamy, *Color Res. Appl.*, 1992, **17**, 142–144.
57 I. Gupta, P. Kumar, S. Singh, S. Bhagwan, S. K. Chhikara and D. Singh, *Inorg. Chim. Acta*, 2022, **543**, 121183.
58 I. Gupta, S. Singh, S. Bhagwan and D. Singh, *Ceram. Int.*, 2021, **47**, 19282–19303.
59 R. G. Hunt, *In TV and Video Engineer's Reference Book*, Butterworth-Heinemann, 1991, p. 9-1.
60 S. Sharma, N. Brahme, D. P. Bisen and P. Dewangan, *Opt. Express*, 2018, **26**, 29495–29508.
61 K. Nehra, A. Dalal, A. Hooda, S. Singh, D. Singh, S. Kumar, R. S. Malik, R. Kumar and P. Kumar, *Inorg. Chim. Acta*, 2022, **539**, 121007.
62 R. Reisfeld, *Rare Earths*, 2005, 65–97.
63 S. Dalal, D. Singh, A. Hooda, S. Redhu, S. Malik, V. Aggarwal, S. Kumar, R. S. Malik, P. Kumar and J. Sindhu, *Opt. Mater.*, 2024, **150**, 115159.
64 J. Donaldson and G. V. Williams, *Int. J. Nanotechnol.*, 2017, **14**, 558–565.
65 S. Biju, D. A. Raj, M. L. Reddy, C. K. Jayasankar, A. H. Cowley and M. Findlater, *J. Mater. Chem.*, 2009, **19**, 1425–1432.
66 H. Yu, Q. Liu, J. Li, Z. M. Su, X. Li, X. Wang, J. Sun, C. Zhou and X. Hu, *J. Mater. Chem. C*, 2021, **9**, 562–568.
67 S. Malik, K. Jakhar, D. Singh, A. Hooda, K. Nehra, S. Kumar, R. S. Malik and P. Kumar, *J. Mol. Struct.*, 2024, **1311**, 138334.